

Simulation of Foaming and Deformation for Composite Aluminum Foams

H. Bayani and S. M. H. Mirbagheri*

Department of Mining and Metallurgical engineering, Amirkabir University of Technology, Tehran, Iran

Abstract: In this study, the rupture criterion of bubbles wall in Aluminum metal foam liquid was investigated at the first stage, using Lattice Boltzmann. The two phases modeling were accomplished by using a modified Shan-Chen model. This model was run for several bubbles in A356+3wt.%SiC melt system. Then, bubbles morphologies (virtual metallographic) for A356+3wt.%SiC foams were simulated. Results showed that simulation data and the virtual metallographic have a good agreement with the metallographic empirical results after solidification. In the second stage, several cubic A356+3wt.%SiC foams were compressed under uni-axial compression load based on ASTM E9 standard. Stress-strain curves of foams were determined by a data acquisition system gaining 10 samples per second. Foams plastic deformation behavior then was simulated based on a new asymptotic function using ABAQUS software. Discretized digital solid-model of the solid bubbles was prepared with virtual metallographic images which obtained from the present code. The load-displacement curves were then plotted for simulation and experimental results. Results show that both curves which were obtained from experimental and simulation have a good agreement with approximately 1.8% error. Therefore, the present software could be a useful tool for predicting the metal foams plastic deformation behavior without any experimental try and error.

Keywords: Metal Foam Aluminum A356, Lattice Boltzmann Method, Shan-Chen model Plastic deformation, mIR asymptotic model

1. Introduction

New technologies increase the demand for advanced materials. Today, metal foams gained a lot of interest as one of the major branches of advanced materials. Metal foams are known for their unique physical and mechanical properties, including high stiffness while having low density and high compressibility with good energy damping capability. This consideration has made metal foams very interesting for researchers in both scientific and industrial communities in the recent years and several methods and procedures have been developed to produce them [1-4]. Metal foams generally can be classified into two basic categories: closed cell foams and open cell foams. Although these methods are practically quite different, the resulting metal foams, especially in case of mechanical behaviors exhibit many similarities. The main difference is in the geometry of porous foam or their so called cellular structure. This distinction makes different applications for each category, for example, while open cell-foams might be attractive for filtering applications because of their ability to pass fluid through their porous structure, closed-cell foams cannot be used for such proposes. Closed cell foams are mostly consumed in industries dealing with impact, noise and energy absorption while most open cell foams are used in heat/ion exchangers, filtration and similar industries. Despite the advantages, the employment of metal foams in industrial applications is limited due to production difficulties such as the inhomogeneity and poor reproducibility of foam structures [5]. The foams are quite stable in the absence of external factors but bubbles stability and energy balance in cell structures would be considered as first challenges in production procedure. To

overcome these difficulties, one should consider improving the governing mechanisms according to the understanding of basic physical phenomena occur during metal foam formation. Now the main problem appears: in metals, unlike ionic liquids, the mechanisms involved in the metal foam formation are not yet fully understood. It is generally accepted that formability of metal foams is intimately correlated with the presence of particles [6]. Bubble stability is the primitive challenge in understanding the base mechanism of metal foam formation. A variety of studies and researches have been done by scientists in order to investigate and analyze the parameters affecting bubble stabilization. Most of this investigation focused on ionic liquid environment, especially in water, with no impurity, studying single bubble dynamics. But in metal foams, one is involved with a metal melt environment as the base liquid of bubble formation, containing dozens of different impurities, even in the purest state. There are three major approaches to study metal foam formation basic mechanism and theories: experimental approach, computational approach and hybrid experimental-computational approach [7]. Simulating bubbles and voids in simple and complex fluids and in material systems has always been a challenging problem using conventional fluid dynamical methods. Different approaches are available for bubble simulation and each has its own strengths and weaknesses. These approaches include: Computational Fluid Dynamics (CFD) [7], Shallow Water [8], Lattice Boltzmann Method (LBM) [9, 10], Discrete Particle, and Cellular Automata (CA) [11]. The Lattice Boltzmann simulation can be used to more accurately simulate the kinetic effects on bubbles [12]. The Boltzmann equation is valid in principle over a wider range of flow physics than the NS equations. An important advantage of the LB approach compared to conventional CFD methods is in its local character, means there are no global systems of equations which have to be solved. The computation time has linear relation with the system size. In addition, boundaries in simulation domain do not have an effective impact on the computation time. These features are essential for foam formation simulation regarding the complex internal structure of foams [6]. Unlike conventional schemes (such as finite element or finite difference methods) that are based on discretization of continuum and macroscopic equations, the Lattice Boltzmann method models the microscopic and mesoscopic kinetic equations. The fundamental idea of LBM is to construct simplified kinetic models that incorporate the essential physics of microscopic or mesoscopic processes so that the macroscopic averaged properties obey the desired macroscopic equations [12].

The aim of this investigation is simulation of foaming process and then simulation of plastic deformation of metal foams. Lattice Boltzmann method is utilized to simulate the two phase system of gas bubbles and metal liquids. In metal foam systems, the particles of disperse phase have interaction in the layers of continuum phase, primarily known as *Thin Liquid Films* [13]. The condition, where the rupture and destruction of thin films is occurred, is a challenge in field of multiphase numerical modeling [14, 15]. The bubbles and their thin walls will control plastic deformation behavior of metal foams [16]. There are several papers for calculating or simulating the thin film or thickness of bubble walls [17, 18]. Impurities in the metal melts play important role in this inefficiency. Thus, a new criterion is required for metallic and non-aqueous solutions in order to model such multiphase systems. In this study, a new criterion is introduced, using the second derivatives of the pressure profile formed between two bubbles, which would have great results as combined with other modeling techniques [19, 20].

On the other hand, generally compressive stress-strain curve of the metal foam has three zones including: elastic deformation, plastic deformation with low strain-hardening up to the densification strain, and hard plastic deformation [21]. However, for dense metals (not metal foam) deformation can be approximated by $\sigma = k\varepsilon^n$. Parameters K and n depend on the material characteristics and describe the strength and strain hardening. However, for metal foams, modeling of strain-hardening is very complex. In metal foams and their composites, n and K are not constant. Despite the fact that a number of research works are dedicated to such studies, still many parameters remain unknown. Therefore, in the present

work, the plastic deformation of Al-Si composite foam, under static uniaxial compression loading is investigated as well. In this study, an asymptotic equation is used for modeling plastic deformation of metal foams until the densification strain.

2. Mathematical Modeling

To develop the new criterion, a two phase LB simulation is performed on two adjacent and growing bubbles. The modified Shan-Chen model prohibits the bubbles of being merged instantly. The thin film formed between the bubbles becomes thinner as the growth continues. In order to investigate the rupture conditions and jointed bubbles, we focused on the pressure gradients and velocity field in the thin film (thin channel). The interaction of the capillarity effect and drainage in this channel, leads to instability during bubbles growth, causes them to be jointed. When the instability appears, the channel (wall) thickness is calculated according to Table 1 and is compared with experimental results and mathematical models predictions to verify the modified Shan-Chen model.

Table 1. Experimental results of minimum cell wall thickness [20].

Alloy	min thickness (μm)
Al	100
AlSi2	80
AlSi7	52
AlSi10	60-70
AlSi12	80
AlSi6Cu4	51
AlSi10Mg0.6	30-50
AlSi12Mg0.6	60-80

2.1. Thin film formation

Lattice Boltzmann method includes two stages in a single time step and different schemes to simulate multiphase systems, including the Shan-Chen scheme. In Shan-Chen algorithm, each phase is considered in a separate lattice (grid), i.e. two separate simulations are carried out simultaneously for a two-phase model. For this purpose, two identical lattices with the same parameters are required, one includes the first phase and the other includes the second phase. Each time step is divided to stream and collision stages and the computations are performed on each lattice independently, as two separate single-phase simulations. However, after two time steps, the Shan-Chen model applies some modifications to the joint points of the lattices, causes them to be coupled at this points. This modification creates new interfaces and prepares the model for the next time step (Fig. 1). If more than one island of the second phase exists in the domain of first phase, there would be no problem in the model as long as no coalescence occurred between them and therefore the predictions are with a good agreement with the real physical behaviors of the second phase. When an overlap occurs, the situation is different. In the first stage of time step, which is the stage of applying streams and collisions, the corona of the bubbles contacts each other, while there is no interference in the fluid domain. The interference causes the bubbles to have direct impact on each other, but this condition is in contradiction with the fact that each interaction of the bubbles is only performed through the fluid domain. Hence data of the overlap zone must be kept separately. So as the interaction of the bubbles begins, the coronas are overlapping and consequently there would be regions in the second phase lattice which have more than single Boltzmann data. If this data is stored in a single container (variable), the behavior of bubbles would be unacceptable. But if one uses separate containers to store the simulation data of each bubble independently, the result will be appropriate (Fig. 2). The main challenge is computing the Shan-Chen parameters in the interaction zone due to the presence of data of multiple

interacting bubbles (which is not a problem for one bubble model because it is only coupled with a single fluid data). Each data is related to its corresponding bubble and its corona, e.g. with two interacting bubbles, we have three data sets in the interaction zone, one for fluid domain and two others for each bubble. Equilibrium bubble velocity equation is as follows [22]:

$$u_{i\text{gas}} = u_{\text{total}} + \tau_{\text{gas}} (F_{\text{gas}} - G \xi_{i\text{melt}}) \quad (1)$$

where $u_{i\text{gas}}$ is bubble i velocity in gas lattice, $u_{\text{tot}} = (u_{\text{gas}} + u_{\text{melt}})/\Sigma\rho$, τ_{gas} is gas lattice relaxation time, F_{gas} is external force for gas lattice, G is interaction strength, and $\xi_{i\text{melt}}$ is partial pressure in fluid lattice point which is unique. The fluid velocity could be calculated using the following equation [22]:

$$u_{i\text{melt}} = u_{\text{total}} + \tau_{\text{melt}} (F_{\text{melt}} - G \xi_{i\text{gas}}) \quad (2)$$

where $u_{i\text{melt}}$ is melt velocity in fluid lattice, τ_{melt} is fluid lattice relaxation time, F_{melt} is external force for fluid lattice, and $\xi_{i\text{gas}}$ is partial pressure in gas lattice point which has two values in a two bubbles model that could not be cumulated. By increasing the number of bubbles, there would be more $\xi_{i\text{gas}}$ in the interaction zone. The second condition is related to the barrier wall (thin film) formed between the bubbles, that determines which $\xi_{i\text{gas}}$ should be used in each point of the interaction zone. Hence the velocity values are zero on the barrier wall (the location of the barrier wall depends on the size, shape and initial velocity of the bubbles but certainly the velocity of the bubbles are equal on the barrier wall), but in the regions close to the first bubble, the $\xi_{i\text{gas}}$ of the first bubbles is incorporated in the calculations. This rule is applied to the calculation of the velocity in every point of the interaction area according to their closest bubble. This novel condition leads to the formation of the barrier wall spontaneously and the incorporated bubbles will never merge. This computational process is presented schematically in Fig. 3. Now another criterion is required to determine the time of decay of barrier wall (thin film rupture). In the present investigation, this criterion is developed using the second derivative of the pressure profile across the interaction zone to disable the above algorithm and let the bubbles merge.

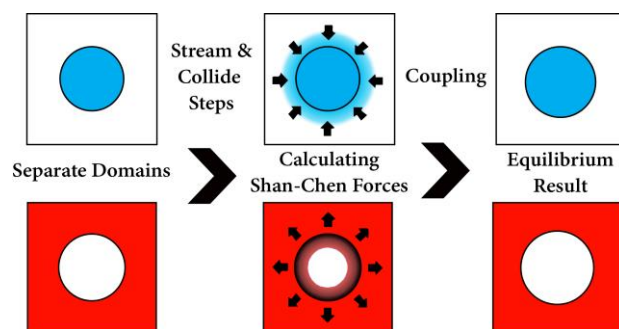


Fig. 1. Shan-Chen simulation steps of single bubble as the second phase.

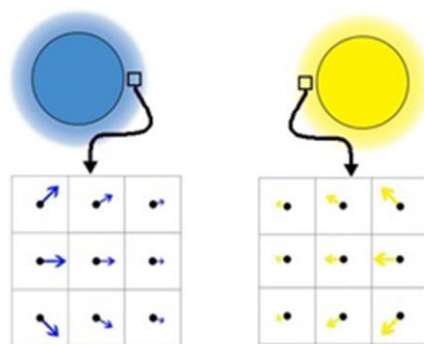


Fig. 2. Interaction of bubble coronas and existence of multiple data.

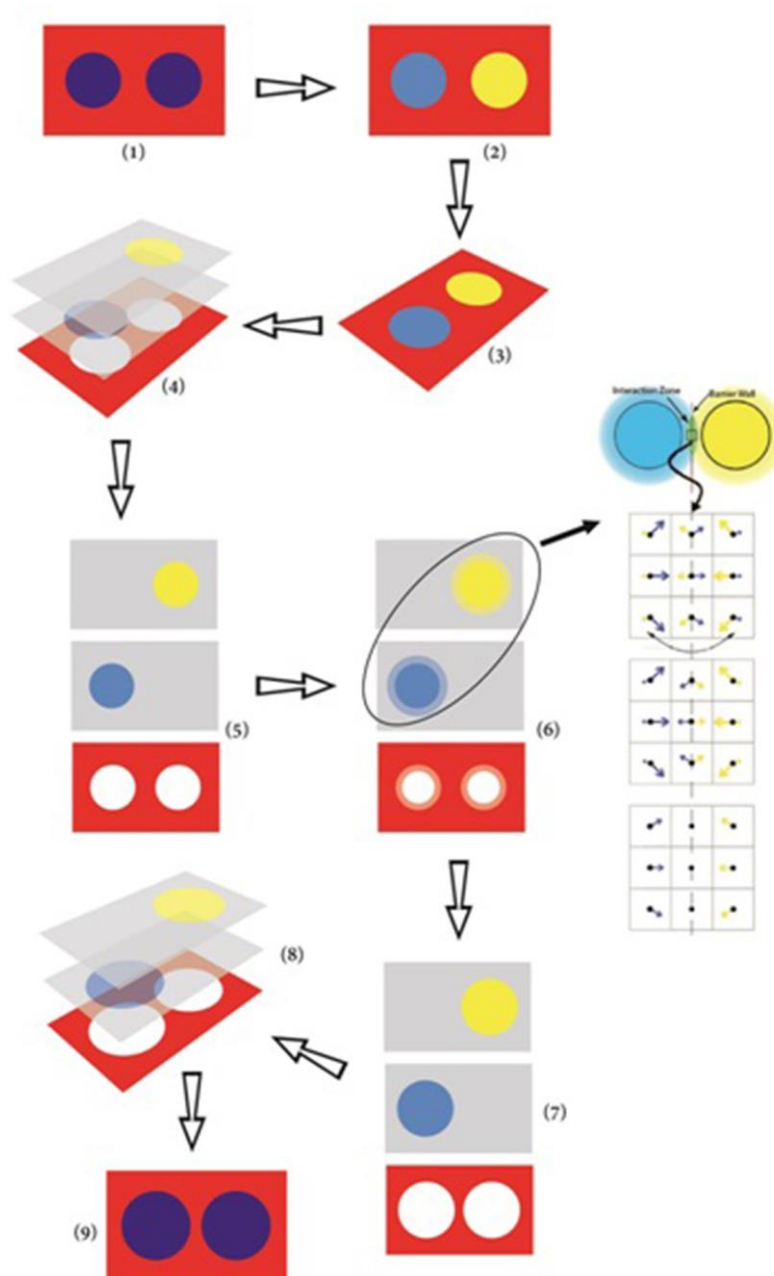


Fig. 3. Schematic demonstration of simulation steps: 1) Initial state of computational lattice with two gas bubbles 2) separating the second phase grid 3,4,5) placing each bubble in its own lattice and fluid in a separate lattice 6) computing the velocities across the grid which leads to the formation of the coronas, and then coupling the lattices and calculating the interactions in the interaction zone using the new algorithm 7) computing the new size of the bubbles and update the fluid domain 8,9) merge the lattices to postprocess the final output.

2.2. Thin film rupture

Thin channel rupture phenomena would be described in two different mechanisms. One of these mechanisms is the nucleation of a void and its growth due to surface tension forces. In this theory, in micro scale, a hole is formed randomly in the thin channel and void formation energy becomes negative according to the follow equation [19]:

$$\begin{cases} \Delta G_{void} = 2\pi\Gamma r - 2\pi\gamma r^2 < 0; & r > r^* = \frac{\gamma}{2\Gamma} \\ \Delta G_{void} = 2\pi\Gamma r - 2\pi\gamma r^2 > 0; & r < r^* \end{cases} \quad (3)$$

However, in radii less than the critical value (r^*), the void would be removed. Thus, this mechanism requires activation energy $E_a = E(r^*)$ to start, i.e. the nucleation of void is a thermal activated mechanism and could be described by Arrhenius equation [19].

The second mechanism, considers a kind of instability similar to Spinodal decomposition. In this mechanism, if the thickness of the thin channel falls below a critical value due to drainage, a perturbation occurred. Now the instability in the thin film is appeared as the wavelength of this perturbation exceeds the critical wavelength, which leads to the rupture of the film. This critical wavelength would be calculated as below [19]:

$$\lambda_c = \sqrt{\frac{-2\pi^2\gamma}{d^2V/dh^2}} \quad (4)$$

where γ is the surface energy and $V(h)$ is the free energy of interface as a function of the thickness. If one considers the thin film as a cylinder with radius R and thickness h which is enclosed by two interfaces with surface tension γ (see Fig. 4), then the critical thickness of drainage would be [19]:

$$h_c = 0.22^4 \sqrt{\frac{AR^2}{f\gamma}} \quad (5)$$

As the thin channel thickness reaches this value, the rupture will occur. The time taken from the instability to the rupture could be calculated as well [19]:

$$\tau = \frac{96\pi^2\gamma\eta h_c^5}{A^2} \quad (6)$$

If the limitation could be neglected, the thickening would continue till the formation of a molecular wall, but in the presence of stabilizer particles, surfactants or oxide films, the situation would be different. The described mechanism is more suitable for rapid growth, in which the system has no surfactant.



Fig. 4. Disk on the interface of bubbles interaction called Interaction Area.

In metal melts, the oxide films and stabilizer particles are presented, which means it's more probable for the second mechanism to occur. Thus one of the objectives of developed code is to model the instability in the thin wall formed between the bubbles. Experimental results of the critical thickness of aluminum alloy cell wall are listed in Table 1 [20]. Previous contributions in the field of thin film modeling are mostly based on this criterion in order to determine the cell wall rupture time. But the critical

thickness depends natively on the size and dynamics of the involved bubbles, i.e. the constant critical thickness criterion is not a well-defined boundary condition to model the thin film formation and destruction. Hence it's crucial to define a new critical thickness criterion as a function of the size of the interacted bubbles. The critical thickness function is rarely investigated in previous researches. In the present study, a novel criterion is introduced to model the thin film more efficiently and to derive a critical thickness function consequently that would be dependent on the size of the bubbles. This function would be based on the dynamics of the fluid in the interaction area along the involved bubbles. The developed criterion is based on the computed pressure in the thin film. Instability is observed in the pressure profile and velocity curves along the thin film as the bubbles get close to each other and the rupture of the cell wall begins to form. Processing the second derivative of the pressure profile in the thin film along the vertical axis leads to the detection of this condition computationally during the numerical simulations of the bubbles growth and coalescence. The second derivative of pressure equals zero at the moment of the instability causes the cell wall rupture, so the criterion would be defined as preventing the bubbles merge till the second derivative of the pressure profile in the middle of the formed thin film reaches zero. Interpolating the results of sequent simulations conducted using this new criterion leads to obtain an improved equation of the critical thickness as a function of the bubbles radius.

2.3. Deformation modeling of metal foam

In order to investigate the deformation behavior during plastic deformation, two Aluminum composites Al-A356+3wt.%-SiC with 25-32 PPI, were prepared based on casting method [12]. Foam samples with square cross-section of 22x22 mm were cut with the height of 1.5 times of their diameters. The uniaxial quasi static loading on the foams were then performed using 25 kN Instron 8502 test machine at a crosshead speed of 2.5 mm/minute and 1.3×10^{-3} (1/sec) strain rate at room temperature. The curves of force-displacement were plotted by a data acquisition system gaining 20 data per second. Then cellular structure of foams was prepared by metallographic test. In the next stage according to Fig. 5, cellular structures obtained from the present software (virtual metallographic images) converted to Solid images by some commercial software's Illustrator, Corel CAD, and Solid Work, respectively, in order to stress the simulation by ABAQUS software. Simulation details are presented in Table 2. In this software, all Solid images of the porous metal were meshed and simulated elastic-plastic deformation of foams. The elastic-plastic behavior of metal foams during uniaxial compression was conducted based on the following equation (mIR model) [21]

$$\sigma = I_0(1 - R\varepsilon)^{-m} \quad 0 < m < 1 \quad (7)$$

where m , I_0 , and R are the foams strain-hardening exponent, the crushing start stress (MPa), and the function of strain rate ($R=1$ in this investigation), respectively. It is noticeable that mIR plastic deformation model is not valid for data next to the asymptote line ($\varepsilon = 1$). Also, it was ignored from elastic deformation during compression, because in metal foams the elastic energy values are negligible in contrast to plastic energy. Due to asymptotic nature of the mIR model, this could use in ABAQUS software for stress analyzing. Finally, curves load- displacement obtained from compression simulation were compared with the experimental results obtained from data acquisition system. Also virtual metallographic and real (experimental) metallographic images were compared.

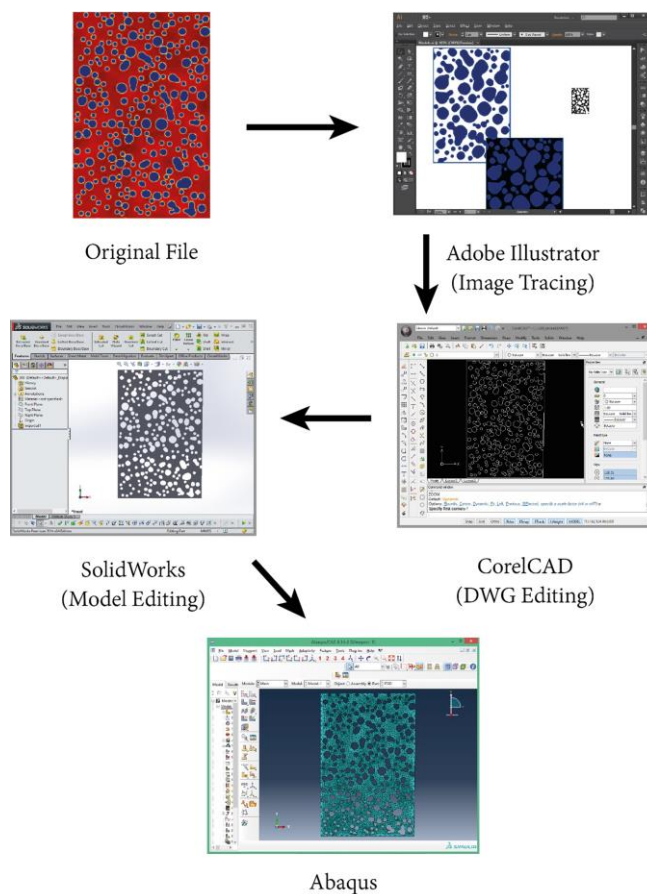


Fig. 5. Transfer sequences present code output to Solid format for ABAQUS software due to plastic deformation simulation.

Table 2. Deformation simulation details for ABAQUS 6.14.

Material properties	
Material	Aluminum A356
Young module	70×10^9 Pa
Poisson's ratio	0.33
Plastic Deformation	mIR model
Density	2700 kg/m^3
Damage model	Shear damage
	Ductile damage
	MSFLD damage
Meshing properties	
Mesh type	2D triangular
	Explicit
	Plane Stress
Mesh code	Linear
	CPS3
Boundary condition	
Left and Right	Displacement in X direction = 0 ($U_x = 0$)
Bottom	$U_x=0, U_y=0$
Top	$U_y=-0.035$
Simulation solver	
Step	Dynamic Explicit
Interactions	
Interaction type	General contact
Interaction property	Normal behavior (hard contact)

3. Results

Simulation results of two bubble interaction in aluminum melt is shown in Fig. 6. Using modified Shan_Chen model for multiphase simulation leads to more acceptable result that is presented in Fig. 7. Figure 8 demonstrates the instability in pressure and velocity distribution at the moment of cell wall rupture. Further simulations of bubbles with various radiuses were conducted and bubble radius, thin film radius (interaction area) and thin film thickness were recorded in each simulation at the moment that cell wall instability happened. The results are plotted in Figs. 9 and 10. By fitting a curve on the data in Fig. 9, new equation (Eq. (8)) is derived to demonstrate the relation of bubbles radius and thin film radius.

$$R_b = 2.088 \ln(r) + 0.114 \quad (8)$$

where R_b is the radius of interaction area and r is the radius of bubbles. Consequently, two improved equations would be interpolated from Fig. 10 data for the critical thicknesses in aluminum melt (Eqs. (9) and (10)):

$$h_c = 0.03R_b^{0.45} \quad (9)$$

Equation (10) is a second order equation that is fitted on simulation results and can be applied for cell wall critical thickness calculation in aluminum A356 foams.

$$h_c = 0.002R_b^2 - 0.003R_b + 0.035h_c \quad (10)$$

And finally in order to have an equation similar to Eq. (5), the interpolation of simulation results would describe the critical thickness of cell wall in the following form:

$$h_c = 45.2^4 \sqrt{\frac{AR^{1.826}}{f\gamma}} \quad (11)$$

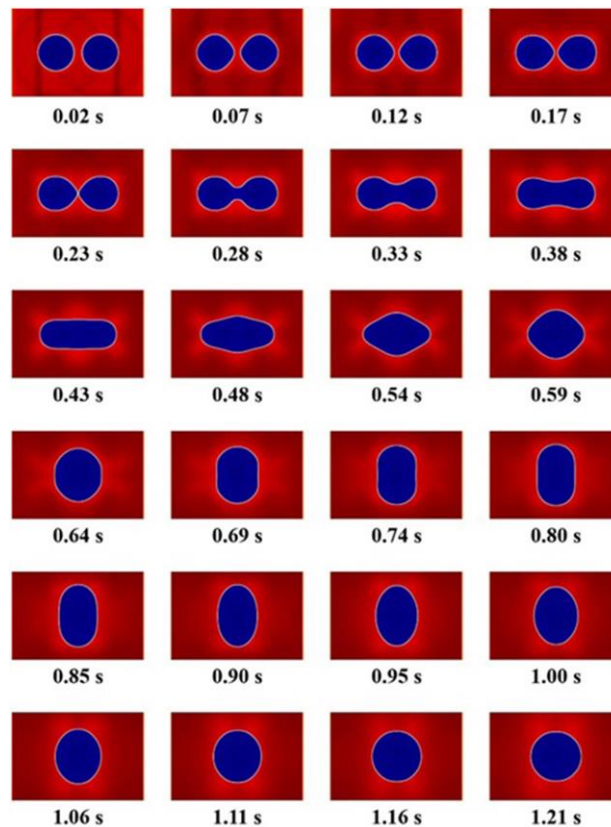


Fig. 6. Simulation of two inline bubbles by LB method and Shan-Chen multiphase model in OpenLB open source code.

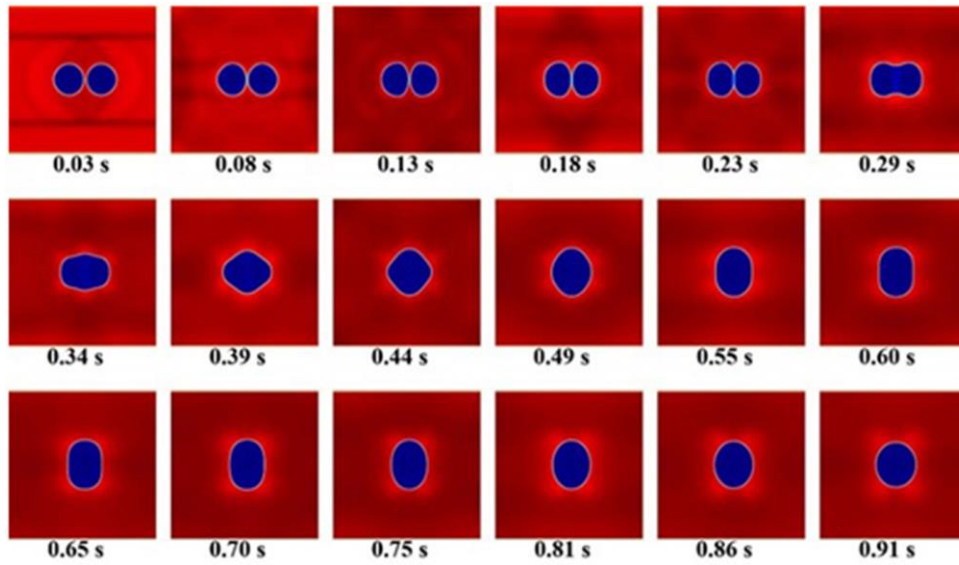


Fig. 7. Coarsening simulation of two in line bubbles by LB method and modified Shan-Chen multiphase model in OpenLB.

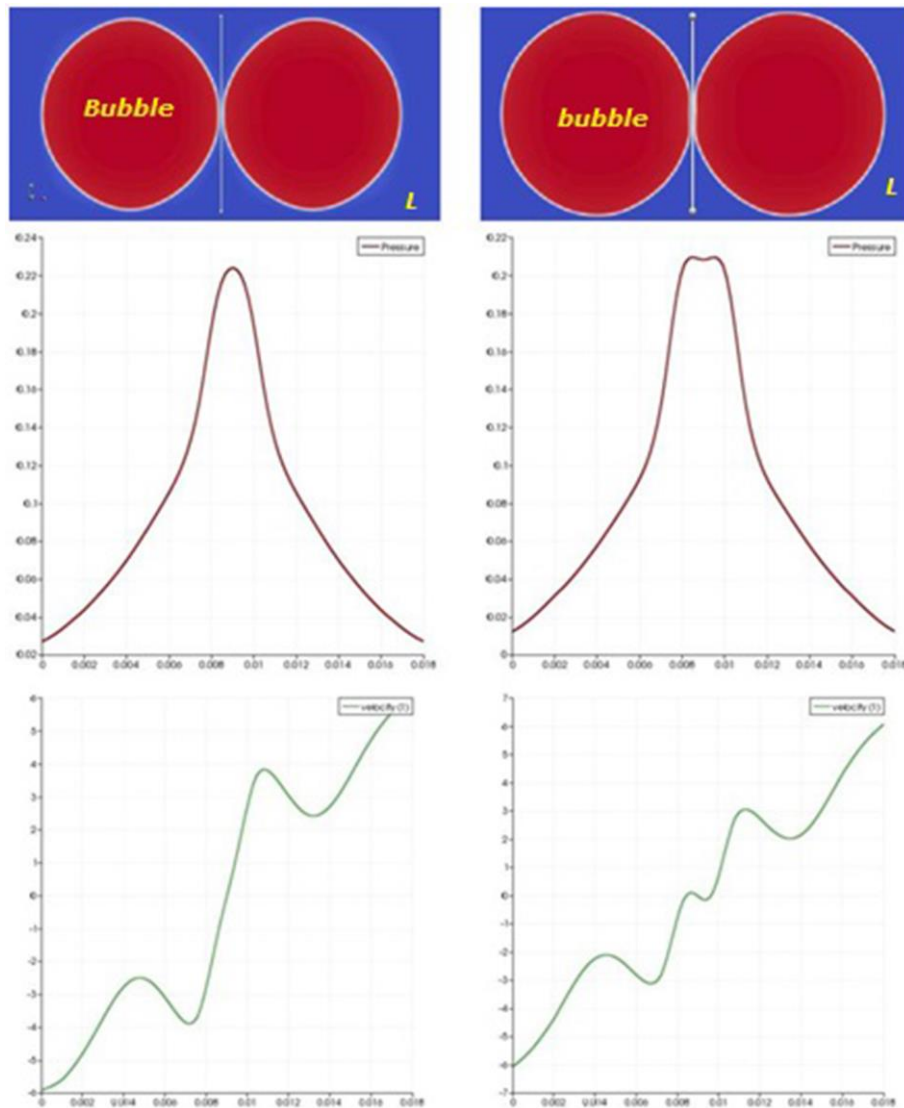


Fig. 8. Plot of pressure and velocity across a vertical line in the middle of two bubbles. Left: before instability, Right: after instability. Red line indicates the pressure and green line is vertical velocity.

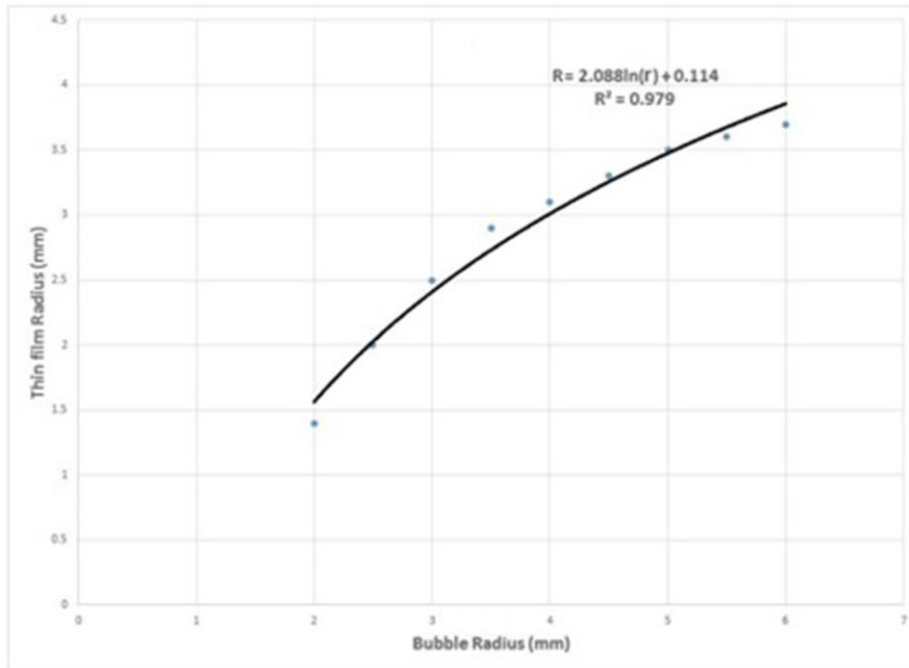


Fig. 9. Curve fitted on simulation results for thin film disk radius versus bubbles radius.

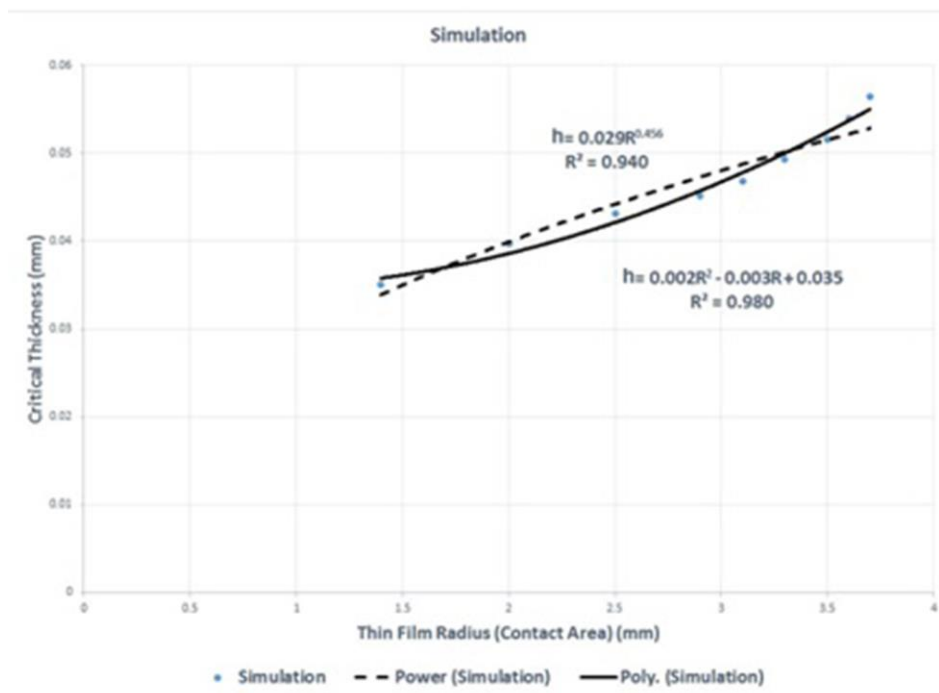


Fig. 10. Curve fitted on simulation results for critical thickness versus thin film disk radius.

Figure 11 shows the comparison between the results of modified Shan_Chen multiphase simulation using the second derivative criterion and the cross section of a mounted aluminum A356+3wt.%SiC metal foam. Figure 12 shows results of compression experimental test and simulation test during compression by ABAQUS software based on the method in Fig. 5. Also for quantitative comparison, Fig. 13 plotted the stress strain curves that obtained from simulation and experimental test.

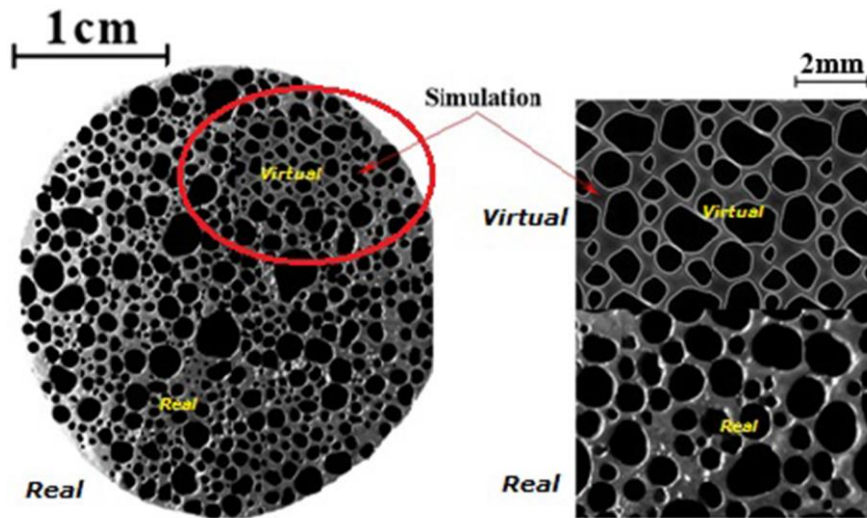


Fig. 11. Real and virtual metallographic structure of porous aluminum metal foam.

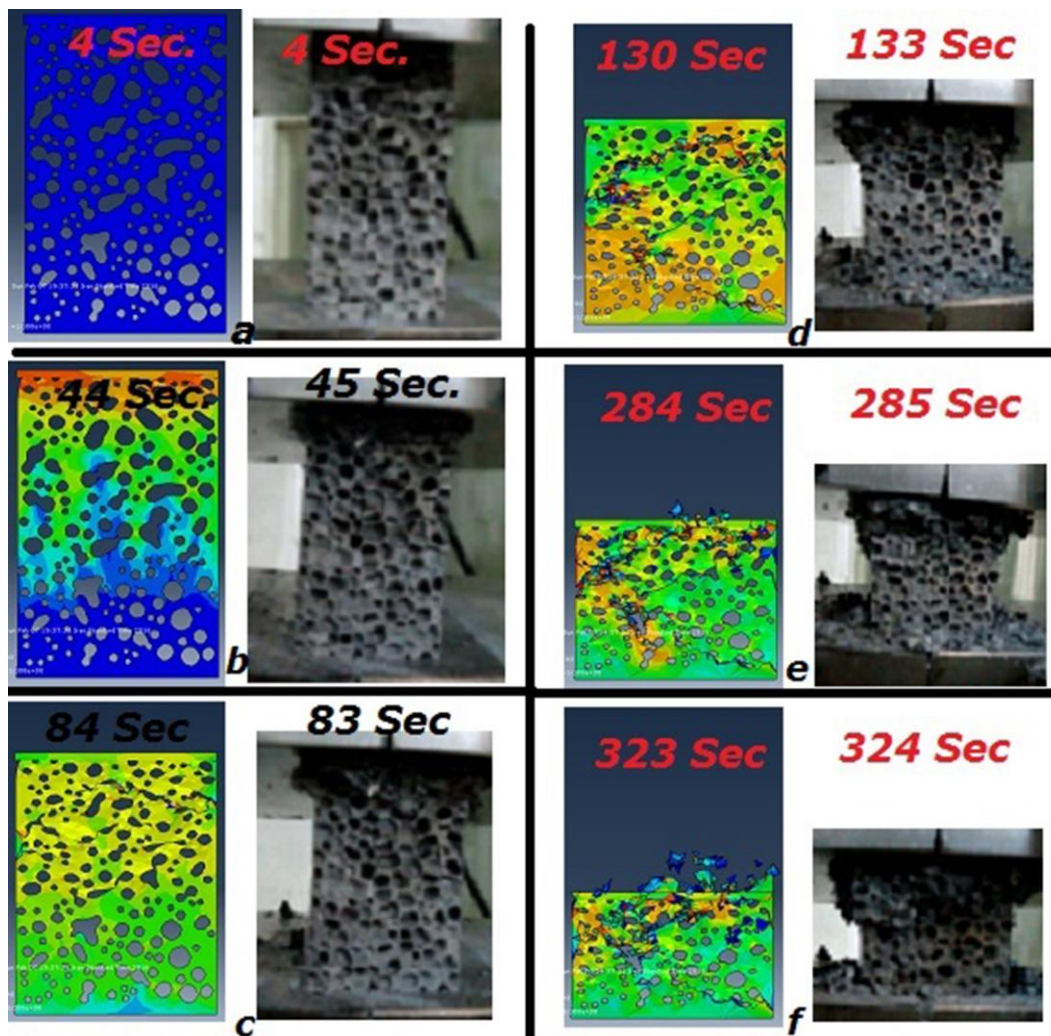


Fig. 12. Qualitative comparison between plastic deformation simulation and experimental for A356+3wt.%SiC foam during compression test with 1.3×10^{-3} (1/sec) strain rate.

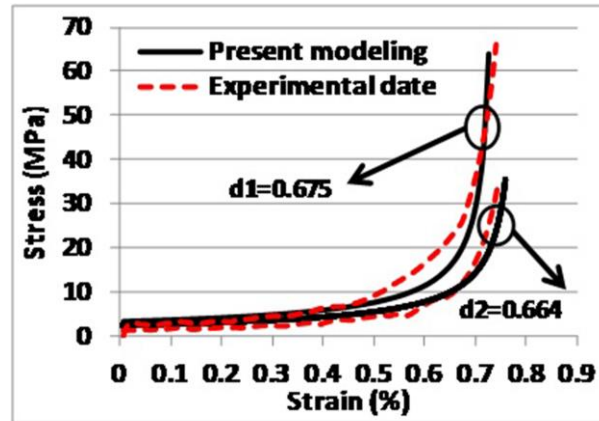


Fig. 13. Quantitative comparison between obtained stress-strain curves from simulation and experiment for A356+3wt.%SiC foams with two different densities.

4. Discussion

If the growing bubbles in the aluminum melt are in a domain with infinite degree of freedom in motion, they would take more distance in which the velocity field caused by their growth will not coalesce, and in case of a limited domain, the appeared thin wall between them begins to become thinner. The presence of capillary forces would cause the geometry of the bubbles not to remain in spherical shape and the interface would be relatively flat. Shan-Chen model is not fully capable of simulating this phenomenon, so special modifications are necessary to model the thin film formation. In unmodified version of this scheme, the simulation result would be similar to Fig. 5. However, as mentioned earlier, the thin film is formed in metal melts. By modifying the original Shan-Chen scheme and applying the second derivative criterion, the approaching and merging of the bubbles would be similar to Fig. 6 and has a good agreement with experimental investigations. By considering and analyzing the pressure gradients along the thin film in this condition, an instability in pressure profile is observed in a thickness that seems to be independent of the bubble size (Fig. 8). In a mathematical point of view, the maximum point in the pressure gradient curve will change to an inflection point, which means the second derivative of pressure gradient is zero. This instability causes a condition like Spinodal decomposition in the thin film which leads to the sudden rupture of the cell wall. Similar behavior would be observed in velocity curve. Previous investigations on critical thickness for aqueous solution demonstrate the dependency of this thickness to Eq. (5). The results of the simulation performed using the second derivative criterion is considerably interesting. Primarily the results of bubbles coalescence in different sizes indicate the existence of a dependency between the interaction area and the radius of the bubble, and the value of this dependency decreases by the bubble radius increment. This tip is rarely considered in experimental investigations due to the measuring complexities. Furthermore, the relation of thin film thickness and the radius of interaction area have a good agreement with experimental data. Gathering the results of the simulations and interpolating a curve similar to Eq. (5) on the outputs indicate that an improved equation would be derived for the critical thickness in aluminum melt. The relation between radius of interaction area and critical thickness of cell wall is not exactly determined yet, however, Manev and Nguen have explained it in their review paper about microscopic thin films in aqueous solutions. They have reported that the proportion is less than $R^{0.5}$ in Eq. (5). This value is more than experimental data ($R^{0.13}$) due to the simplification assumptions [13]. They also reported that the power of R may be between 0.1 and 0.34, depending on many complicated parameters such as intermolecular forces and surfactants. Scheludko [14] has proposed an equation that describes the outflow of fluid from interaction area. By using this equation and Manev investigation,

critical thickness would be proportional to $R^{0.4}$, and in present research by using the simulations results and considering the different intermolecular forces in aluminum alloy molten metal, the critical thickness is estimated proportional to $R^{0.46}$. It's worth noting that the data indicate the thickness of the thin film is proportional to $R^{0.46}$, and this would be different from the Eq. (5), but has acceptable accordance with the results of Manev and Nguen [13], which was based on the results of various investigations in this field. Hence, the results of the performed simulation have an acceptable accuracy according to experimental data (Table 1) and the developed code and the second derivative criterion show good performance in modeling the rupture of the thin film. Therefore, the Eq. (5) would be rewritten for metal melts as Eq. (8). Increasing the number of points in the interpolation leads to a better equation. The second order equation is represented in Eq. (9). This equation demonstrates that the thickness of the thin film could not be less than a specific value. Furthermore, increasing the radius of interaction area, which depends on the size of bubbles, causes an increment in stable wall thickness. Here, if the presence of impurities or stabilizers could prevent the thinning of the wall, the rupture would be delayed. This interruption will continue until the thickness of stable wall become more than the thickness of real wall due to the increment in the radius of interaction area, which is a subsequent effect of bubbles volume increment. In this situation, the instability will appear and the rupture of the wall begins. Thus, the final structure of the metal foam would be created by expanding the modeling to a domain with more bubbles and continuing the simulation until the first coalescence occurs. As shown in Fig. Fig. 1 by considering the random nucleation and growth in the simulation domain, the results would be closer to real metal foam structure images. Figure 11 show that the simulation metallographies of metal foams (virtual) are very similar to real metallography images. Therefore, we can import these images as Solid-work format based on Fig. 5 in the ABAQUS software in order to stress analyzing. However, metallic foams examined in this work are as composite (A356+3wt.%SiC). Therefore, they are expected to show nonlinear strain-hardening during plastic deformation. To start, seem a good approximation would be $\sigma = K\varepsilon^n$ equation for metallic materials (dense materials). However, this model ($\sigma = K\varepsilon^n$) looks to be not sufficiently precise for metal foams (porous material) because of it cannot present the strain hardening behavior of both foams using the same parameters. Several parameters are needed for modeling of the strain-hardening which depend on the absorption energy curves [21]. Therefore, in this investigation mIR model was used based on Eq. (7) and simulation stress analyzing was achieved by adding the obtained metal foams from the method in Fig. 5. The simulation results of stress distribution and deformation stages then were plotted near the experimental results in Fig. 12. According to Fig. 12, the plastic deformation of A356+3wt.%SiC foam was started from top of the sample during uniaxial compression, the plastic deformation concentrates in a layer with certain thickness while the rest bears elastic deformation only in this moment. Moreover, crashing was started from top of the sample foam and the crashed-layer progresses toward bottom during compression. In fact, density of foams from approximate 0.67g/cm³ during deformation will be densified to 2.7 g/cm³. Curves of Fig. 13 illustrates the mIR plastic deformation model results for two A356+3wt.%SiC foams with densities 0.664 and 0.675, respectively. In this figure, simulation and experimental results (with 1.3x10⁻³ (1/sec) strain rate) indicate that the predicted plastic stresses (plateau stress region in Fig.15) by using Eq. (7) have a good agreement with 1.8% error. It should be mentioned that the predicted plastic stress of metal foam is dependent on strain rate or (R) factor in this model, especially in high strain rates. Fig. 14 shows the obtained stresses results of the mIR model and experimental stress for several foam with various densities at densification strain $\varepsilon = 0.75\%$. Therefore, validity of the mIR plastic deformation model is acceptable for these metal foams.

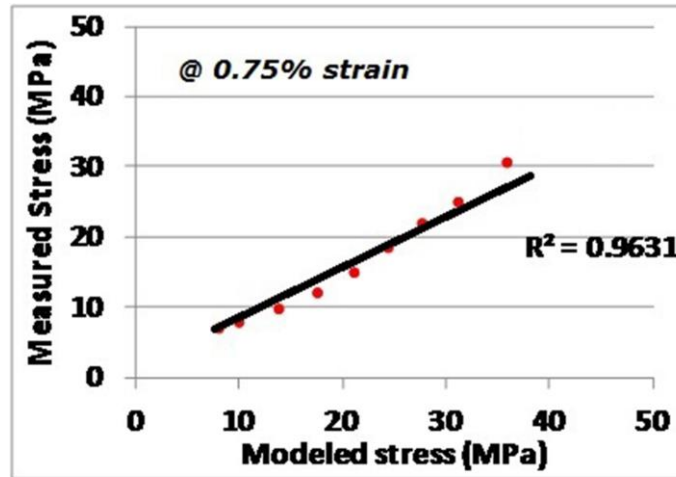


Fig. 14. Validation of metal foams deformation simulation based on Eq. (7) at present work.

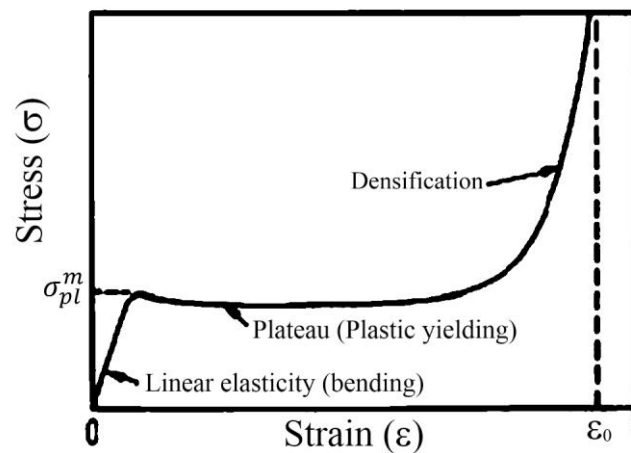


Fig. 15. Schematic of metal foam deformation stress-strain curve and its regions.

5. Conclusion

1. The instability in cell wall of metal foams would be predicted by analyzing the second derivative of pressure profile ($\nabla p=0$) along the thin film.
2. The thickness of stable cell wall doesn't depend on the size of the bubbles.
3. In this investigation, simulation of plastic deformation based on mIR asymptotic model has a good consistency with experimental results having approximately 1.8% error.
4. Plastic deformation behavior for A356+SiC composite foams show crashing process during compression at solid bubbles walls, therefore these foam have a semi- brittle behavior during plastic deformation.
- 5- Present software could produces simulation data which is capable of being linked to the stress analyzer software's such as ABAQUS and COMSOL.

Acknowledgment: This work was supported by the Metal Foam Group of Amirkabir University (MFGAU) through grant 110-mir-1394514-II. Authors are grateful of Rahyaft Advanced Sciences and Technologies Co for their support in casting metal foams.

5. References

- [1] J. Banhart, Manufacturing routes for metallic foams, *Jom*, 52 (2000) 22-27.

- [2] J. Banhart, Manufacture, characterization and application of cellular metals and metal foams, *Prog. Mater. Sci.*, 46 (2001) 559-632.
- [3] J. Banhart, J. Baumeister and M. Weber, Powder metallurgical technology for the production of metallic foams, in *European Conference on Advanced PM Materilas*, ed Brimingham, (1995), pp. 201-208.
- [4] C. Koerner, Integral Foam Molding of Light Metals, Springer, (2008).
- [5] M. Thies, Lattice Boltzmann Modeling with Free Surfaces Applied to Formation of Metal Foams, PhD, University of Erlangen, Nuremberg, (2005).
- [6] C. Korner, Foam formation mechanisms in particle suspensions applied to metal foams, *Materials Science and Engineering A*, 495 (2008) 227-235.
- [7] C. Y. Chow, An Introduction to Computational Fluid Mechanics, Wiley (1979).
- [8] D. P. Playne, K. Hawick and M. G. B. Johnson, Simulating and benchmarking the shallow-water fluid dynamical equations on multiple graphical processing units, (2013).
- [9] B. T. Pearce and K. Hawick, Interactive simulation and visualisation of falling sand pictures on tablet computers, (2013)
- [10] K. Hawick, Visualising multi-phase lattice gas fluid layering simulations, (2011).
- [11] C. Peng, The lattice boltzmann method for fluid dynamics: Theory and applications, Master, EPFL, Switzerland, (2013).
- [12] A. Gupta and R. Kumar, Lattice Boltzmann simulation to study multiple bubble dynamics, *International Journal of Heat and Mass Transfer*, 51 (2008) 5192 - 5203.
- [13] E. D. Manev and A. V. Nguyen, Critical thickness of microscopic thin liquid films, *Advances in Colloid and Interface Science*, 114-115 (2005) 133-146.
- [14] A. Scheludko, B. Radoev and T. Kolarov, Tension of liquid films and contact angles between film and bulk liquid, *Transactions of the Faraday Society*, 64 (1968) 2213-2220.
- [15] A. Vrij and J. T. G. Overbeek, Rupture of thin liquid films due to spontaneous fluctuations in thickness, *Journal of the American Chemical Society*, 90 (1968) 3074-3078.
- [16] B. P. Radoev, A. D. Scheludko and E. D. Manev, Critical thickness of thin liquid films: Theory and experiment, *Journal of Colloid and Interface Science*, 95 (1983) 254-265.
- [17] A. Scheludko, Thin Liquid Films, *Advances in Colloid and Interface Science*, (1967) 391-464.
- [18] E. Manev, R. Tsekov and B. Radoev, Effect of thickness non-homogeneity on the kinetic behaviour of microscopic foam film, *Journal of Dispersion Science and Technology*, 18 (1997) 769-788.
- [19] J. Bibette, F. L. Calderon and P. Poulin, Emulsions: basic principles, *Rep. Prog. Phys.*, 62 (1999) 969-1033.
- [20] H. Stanzick, M. Wichmann, J. Weise, L. Helfen, T. Baumbach and J. Banhart, Process control in aluminium foam production using real-time X-ray radioscopy, *Advanced Engineering Materials*, 4 (2002) 814-823.
- [21] H. Bayani and S. M. H. Mirbagheri, Strain-hardening during compression of closed-cell Al/Si/SiC + (TiB₂ & Mg) foam, *Materials Characterization*, 113 (2016) 168-179.
- [22] N. R. Koosukuntla, Towards Development of a Multiphase Simulation Model Using Lattice Boltzmann Method (LBM), MSc, University of Toledo, Ohio, 2011.

شبیه سازی فرایند فومسازی و تغییر شکل برای فوم آلومینیم کامپوزیتی

حسین بیانی و سید محمد حسین میرباقری

دانشکده مهندسی معدن و متالورژی، دانشگاه صنعتی امیر کبیر، تهران، ایران

چکیده: در تحقیق حاضر ابتدا معیار فروپاشی دیواره حبابها در فوم فلزی آلومینیم با استفاده از ورش شبکه بولتزمان بررسی و مدلسازی دو فازي با استفاده از روش شانچن انجام شد. این مدل برای مقادیر متعدد حبابها در سیستم مذاب آلیاژ $A356+3wt.\%SiC$ اجرا شد. سپس مورفولوژی حبابها (متالوگرافی مجازی) برای فوم $A356+3wt.\%SiC$ شبیه سازی شد و نتایج نشان داد که داده های شبیه سازی و متالوگرافی مجازی تطابق خوبی با نتایج تجربی متالوگرافی پس از انجماد دارند. در مرحله دوم فومهای مکعبی متعددی از $A356+3wt.\%SiC$ تحت فشار محوری بر اساس استاندارد ASTM E9 فشرده شد. منحنیهای تنش-کرنش فومها توسط سیستم ثبت داده با سرعت ثبت 10 داده در هر ثانیه مشخص شد. رفتار تغییر فرم پلاستیک فومها سپس با استفاده از تابع تقریبی جدید توسط نرم افزار ABAQUS شبیه سازی شد. مدل گسسته عددی از حبابهای منجمد با استفاده از تصاویر متالوگرافی مجازی تولید شده از کد حاضر تهیه شدند. منحنیهای نیرو جابجایی برای نتایج شبیه سازی و آزمایشگاهی رسم شد. نتایج نشان داد که هر دو منحنی تعیین شده از آزمایش و شبیه سازی تطابق خوبی با خطای تقریبی 1.8 درصد دارند. بنابراین نرم افزار حاضر میتواند ابزاری مناسب برای پیشبینی رفتار تغییر فرم پلاستیک فومهای فلزی بدون انجام سعی و خطای آزمایشگاهی باشد

کلمات کلید: فوم فلزی آلومینیم A356، روش شبکه بولتزمان، مدل شانچن، تغییر فرم پلاستیک، مدل تقریبی mIR